Mechanistic Studies of NH_3-Assisted Reduction of Mononuclear Cu(II) Cation Sites in Cu-CHA Zeolites

Journal:	*Catalysis Science & Technology*
Manuscript ID	CY-ART-09-2021-001646.R1
Article Type:	Paper
Date Submitted by the Author:	19-Oct-2021
Complete List of Authors:	Wilcox, Laura; Purdue University, Chemical Engineering Krishna, Siddarth; Purdue University, Chemical Engineering Jones, Casey; Purdue University, Chemical Engineering Gounder, Rajamani; Purdue University, Chemical Engineering

ARTICLE

Mechanistic Studies of NH_3-Assisted Reduction of Mononuclear Cu(II) Cation Sites in Cu-CHA Zeolites

Received 00th January 20xx,
Accepted 00th January 20xx

DOI: 10.1039/x0xx00000x

Laura N. Wilcox†, Siddarth H. Krishna†, Casey B. Jones, and Rajamani Gounder*

Cu-exchanged zeolites catalyze various redox reactions including the selective catalytic reduction (SCR) of NOx with NH_3 and the partial oxidation of hydrocarbons. The reduction of Cu(II) cations to Cu(I) by NH_3 alone has been observed experimentally, yet fundamental details regarding the Cu active site requirements, reaction stoichiometry, and reaction mechanism remain incompletely understood. Here, we synthesized model Cu-exchanged chabazite (Cu-CHA) zeolites with varying Cu ion densities and distributions of mononuclear Cu(II) ion site types (Cu^{2+}, $(CuOH)^+$) and studied NH_3-assisted Cu(II) reduction reactions using a combination of spectroscopic, titrimetric, and gas-phase product analysis methods. *In situ* UV-Visible and X-ray absorption spectroscopies were used to monitor and quantify the transient partial reduction of Cu(II) to Cu(I) during exposure to NH_3 (473 K), in concert with titration methods that use NO and NH_3 co-reductants to fully reduce to the Cu(I) state any residual Cu(II) ions that remained after treatments in NH_3 alone for a given time period. The techniques provide quantitative evidence that both mononuclear Cu(II) site types are able to reduce in NH_3 alone, and do so to similar extents as a function of time. NH_3-temperature programmed reduction (TPR) revealed that the reaction stoichiometry of NH_3-assisted reduction forms approximately one equivalent of N_2 per 6 Cu sites, regardless of Cu speciation or density, consistent with a six-electron reduction process whereby two NH_3 molecules react with six Cu(II) species to produce one N_2 molecule and six Cu(I) species. These findings provide new insights into the reaction pathways and mechanisms in which NH_3 alone reduces mononuclear Cu(II) sites in zeolites, which are undesired side-reactions that occur during steady-state NO_x SCR and can unintentionally influence SCR-relevant spectroscopic or titrimetric characterization experiments.

1. Introduction

Cu ions exchanged onto zeolite catalysts behave as redox active sites for a variety of applications including selective reduction of nitrogen oxides (NO_x, x = 1, 2)[1–3] and hydrocarbon partial oxidation reactions.[4–8] In the case of partial methane oxidation (PMO) to methanol, a fraction of Cu(II) sites reduce to Cu(I) upon exposure to methane, and after methanol extraction these Cu(I) sites must be re-oxidized to the Cu(II) state by an oxidant (typically O_2) to complete a catalytic cycle.[9–13] In diesel exhaust aftertreatment systems, copper-exchanged chabazite (CHA) zeolites are used to catalyze the selective catalytic reduction (SCR) of NO_x with NH_3,[1–3,14–18] in which one of the prevalent reactions ("standard" SCR) involves NO and NH_3 as co-reductants of Cu(II) and O_2 as the terminal oxidant of Cu(I):

$$4\ NH_3 + 4\ NO + O_2 \rightarrow 6\ H_2O + 4\ N_2 \quad (1)$$

Standard SCR is typically measured under conditions to resemble lean-burn exhaust, which contains O_2 present in excess (ca. 10 kPa) and NO and NH_3 present in equimolar quantities (ca. 0.03 kPa) at ambient pressure.[1,19,20] At these pressures and at temperatures below ca. 523 K, Cu(II) and Cu(I) ions are fully solvated in ammonia to form copper-amine coordination complexes in the divalent ($Cu(II)(NH_3)_4$, $Cu(II)(OH)(NH_3)_3$) and monovalent ($Cu(I)(NH_3)_2$) states, as determined by density functional theory (DFT)-derived thermodynamic phase diagrams[2] and *in situ* Cu K-edge X-ray absorption spectroscopy (XAS).[2,21,22]

Although the preferred reduction pathway of mononuclear Cu(II) cations during NO_x SCR involves co-reduction by NO and NH_3 to consume one equivalent of NO,[23] the reduction of Cu(II) to Cu(I) may also occur in the presence of NH_3 alone. This NH_3-assisted reduction process may be relevant to steady-state NH_3 oxidation, thought to occur via a redox mechanism whereby NH_3 reduces Cu(II) and O_2 oxidizes Cu(I),[20,24,25] which is an undesired side-reaction during NO_x SCR because it consumes NH_3 without reducing NO[26]:

$$4\ NH_3 + 3\ O_2 \rightarrow 6\ H_2O + 2\ N_2 \quad (2)$$

In situ XAS measurements have observed that a fraction of Cu(II) cations present in pre-oxidized Cu-CHA zeolites begin to reduce to Cu(I) species upon introduction of NH_3.[3,21,27–29] Janssens et al. observed that exposure of pre-oxidized Cu-CHA to NH_3 (0.12 kPa, 473 K) produced a mixture of 25% NH_3-solvated Cu(I) and 75% NH_3-solvated Cu(II) complexes, and that the apparent kinetics of Cu(II)

[a.] Charles D. Davidson School of Chemical Engineering, Purdue University, West Lafayette, IN, USA 47907
* Corresponding author. Email: rgounder@purdue.edu
† L.N.W and S.H.K. contributed equally to this work.
Electronic Supplementary Information (ESI) available: [details of any supplementary information available should be included here]. See DOI: 10.1039/x0xx00000x

reduction by NH_3 alone were slower than Cu(II) reduction by a mixture of NH_3 (0.12 kPa) and NO (0.10 kPa).[21] Borfecchia et al. observed that NH_3 alone (0.12 kPa) reduces a small fraction of Cu(II) sites in Cu-CHA to NH_3-solvated Cu(I) sites at 373 K.[27] While studying the transient reduction of NH_3-solvated mononuclear Cu(II) cations in CHA zeolites by NO and NH_3 (473 K), Jones et al. observed that a fraction (ca. 0.10-0.40) of Cu(II) cations begin to reduce to Cu(I) upon introduction of NH_3 (0.03 kPa), prior to introduction of NO.[3] Marberger et al. observed a mixture of NH_3-solvated Cu(I), NH_3-solvated Cu(II), and zeolite-bound Cu(II) species in Cu-CHA zeolites upon exposure to a mixture of NH_3 (0.1 kPa), O_2 (6 kPa), and H_2O (2 kPa) at 463 K.[28]

Density functional theory (DFT) calculations by Paolucci et al. indicate that ammonia can dissociate via N-H bond cleavage at a bare Cu(II) ion in the 6-MR of CHA, but this study did not evaluate the barriers for N-H bond cleavage or model the reaction pathway to form N_2.[30] The authors calculated an N-H bond dissociation energy of 119 kJ mol^{-1} for NH_3 alone, which is less favorable than NO- or O_2-assisted N-H bond cleavage that occurs with dissociation reaction energies of -9 kJ mol^{-1} and 87 kJ mol^{-1}, respectively.[30] This calculation, however, does not include fully ammonia-solvated Cu(II) and Cu(I) states, but does predict a Bader charge of 1.55 for a Cu-NH_2 complex with residual proton bound to an adjacent Al in the 6-MR, helping rationalize experimental observations that NH_3 alone can reduce Cu(II) to Cu(I). *In situ* electron paramagnetic resonance (EPR) spectroscopy has been used to observe a decrease in Cu(II) content with increasing temperature in the presence of NH_3 as further support for Cu(II) to Cu(I) reduction pathways[31,32] Additionally, Ma et al. reported that mononuclear Cu(II) ions in Cu-CHA zeolites reduce during NH_3-temperature programmed reduction (TPR) in the temperature range 373–673 K, with the formation of 1 N_2 per Cu on samples of low Cu density (<0.3 mmol Cu per g);[31] yet, to satisfy an electron balance, this N_2/Cu stoichiometry requires the formation of 5/2 equivalents of gaseous H_2 per N_2 molecule formed, for which experimental validation and a plausible reaction mechanism are lacking. Thus, the reaction stoichiometry and mechanism of NH_3-assisted reduction of mononuclear Cu(II) to Cu(I) sites, and whether NH_3-only reduction mechanisms prevail for all mononuclear Cu(II) sites, are not well understood.

In this work, we use synthesis and ion-exchange methods reported in our prior work[2,33] to prepare model Cu-CHA samples with varying Al density and Cu density to contain predominantly Z_2Cu sites exchanged at paired framework Al centers (i.e., Cu^{2+}), predominantly ZCuOH sites exchanged at isolated Al centers (i.e., $CuOH^+$), or a known quantity of both mononuclear Cu(II) site types. We report *in situ* UV-Visible spectroscopy and Cu K-edge X-ray absorption spectroscopy to observe and to quantify the extent of reduction of Cu(II) to Cu(I) in the presence of NH_3. These quantities were corroborated with gas-phase product stoichiometry measurements during NH_3-assisted TPR of pre-oxidized Cu-CHA zeolites, and titrimetric methods using known reduction stoichiometries by NO and NH_3 after an initial NH_3 pre-reduction treatment at varying ammonia exposure times. These data provide evidence that the reduction of Cu(II) to Cu(I) by NH_3 alone reduces nearly all Cu(II) species with similar apparent kinetics regardless of sample composition (e.g., Al density, Cu site density, mononuclear Cu(II) speciation between ZCuOH and Z_2Cu cations), in a reduction pathway that forms approximately 1 N_2 molecule per 6 Cu(II) cations reduced.

2. Experimental Methods

2.1 Zeolite Synthesis and Aqueous Cu Ion Exchange

CHA zeolites were synthesized with varying bulk Al content (Si/Al = 9–25) and varying fractions of 6-MR paired Al sites (i.e., 2 Al in a 6-MR, as quantified by Co^{2+} titration) according to methods we have reported previously that involve hydrothermal crystallization using different structure directing agents (SDA) or Al reagents.[33] CHA was synthesized with precursors including sodium as the inorganic SDA cation (introduced via NaOH), N,N,N-trimethyl-1-adamantylammonium ($TMAda^+$) as the organic SDA cation (introduced via TMAdaOH), aluminum hydroxide, and colloidal silica. CHA zeolites containing predominantly 6-MR isolated Al configurations (i.e., 1 Al in a 6-MR) were synthesized using solely $TMAda^+$ as the SDA.[33]

After the desired crystallization time, the solids were recovered and washed with alternating steps of deionized water (18.2 MΩ) and acetone (99.9 wt%, Sigma Aldrich) using 70 cm^3 solvent per g solids. The washing and centrifugation process was repeated until the pH of the supernatant was constant between washes. The final wash step was completed with water to remove any residual acetone. After solids were recovered from centrifugation, they were dried overnight in stagnant air at 373 K. The dried solids were then treated in flowing dry air (zero grade, Indiana Oxygen; 1.67 cm^3 s^{-1}) at 853 K (0.0167 K s^{-1}) for 10 h to remove occluded organic material. Following this treatment to remove occluded organics, X-ray diffraction (XRD) patterns (Fig. S1, SI) and micropore volumes estimated from Ar adsorption isotherms (87 K, Fig. S2, SI) gave results consistent with the CHA framework topology.

The H-form of zeolite samples was obtained after aqueous-phase ammonium nitrate (99%, Sigma Aldrich, 1 M NH_4NO_3, 150 g solution per g zeolite) exchange at ambient temperature for 24 h, followed by washing and centrifugation in deionized water (18.2 MΩ; 70 cm^3 per g solids) five times. The solids were dried overnight in stagnant air at 373 K and then treated in flowing dry air (zero grade, Indiana Oxygen; 1.67 cm^3 s^{-1}) at 773 K (0.0167 K s^{-1}) for 4 h to remove NH_3.

Aqueous NH_4^+ ion-exchange (1M NH_4NO_3, 24 h) followed by NH_3 temperature programmed desorption (TPD) was used to quantify the number of Brønsted acid sites on each sample (Table S1, SI). The number of 6-MR paired Al sites (i.e., 2 Al in a 6-MR) was measured by Co^{2+} titration using aqueous ion-exchange protocols described in our previous reports,[33] validated by the measurement of Co^{2+} ion-exchange isotherms to determine conditions that saturated all 6-MR paired Al sites in CHA, of UV-Visible spectra of Co-zeolites that did not show the presence of Co_xO_y species, and of residual H^+ sites on Co-zeolites by NH_3 titration that yielded a site balance consistent with the replacement of two H^+ sites per Co^{2+} ion.

The Cu-form of zeolite samples was obtained by aqueous ion-exchange of the H-form sample with an aqueous copper nitrate

solution (98%, Alfa Aesar, 0.001-0.2 M $Cu(NO_3)_2$, 150 g solution per g zeolite), and the pH of the exchange solution was controlled to ~4 by dropwise addition of 0.1 M ammonium hydroxide (28-30 wt% NH_3 basis, Sigma Aldrich). The exchange solution was stirred for 4 h at ambient temperature, and the solids were recovered by centrifugation and washed five times with deionized water (18.2 MΩ; 70 cm^3 per g solids). After drying overnight in stagnant air at 373 K, the sample was treated in 1.67 cm^3 s^{-1} of air flow (zero grade, Indiana Oxygen) at 773 K (0.0167 K s^{-1}) for 4 h to remove adsorbed species.

2.2 Characterization Methods

2.2.1 Elemental Analysis

Elemental compositions were characterized by atomic absorptions spectroscopy (AAS) using a PerkinElmer AAnalyst 300 Atomic Absorption Spectrometer or inductively coupled plasma optical emission spectrometry (ICP-OES) using a Thermo Scientific iCAP 7000 Plus Series ICP-OES. The samples were prepared by dissolving approximately 0.020 mg of zeolite in 2 g of hydrofluoric acid (48 wt%, Sigma Aldrich), followed by a dilution with 50 g of deionized water (18.2 MΩ). [*Caution: use appropriate personal protective equipment, ventilation, and engineering controls when working with HF.*] Samples analyzed by ICP analysis were further acidified with 2.5 g of HNO_3 (70 wt %, Sigma-Aldrich) before analysis. Elemental compositions of Cu and Al were determined from calibration curves generated by elemental analysis standard solutions. The Si/Al ratios were determined using the Al weight fraction together with the unit cell formula for Chabazite.

2.2.2 Diffuse Reflectance UV-Visible Spectroscopy

Diffuse reflectance UV-visible spectra were recorded using a Varian Cary 5000 UV-Vis-NIR Spectrophotometer attached with a Praying Mantis diffuse reflectance accessory. Baseline spectra were recorded using the parent H-CHA as a 100% reflectance reference material. The sieved (180-250 µm) Cu-CHA was held in dry air (commercial grade, Indiana Oxygen; 5.6 cm^3 s^{-1} g^{-1}) while increasing the temperature from ambient to 723 K (0.167 K s^{-1}) for 2 h. The sample was then cooled to 473 K under the same oxidizing atmosphere and spectra were recorded at this temperature. Following the oxidation treatment, 0.042 kPa NH_3/He (3.0% NH_3/Ar, Indiana Oxygen, diluted with UHP Helium, Indiana Oxygen) was introduced in the presence of flowing air at 473 K. Once the Cu sites were solvated in ammonia, taken as the point at which measured spectra remained unchanged (typically 1 h), air was removed from the inlet stream and spectra were recorded as a function of time at 473 K during NH_3-assisted reduction. After up to 20 h in flowing NH_3, NO (0.042 kPa) was added to the gas stream to monitor the complete reduction of Cu(II) to Cu(I) at 473 K.

To quantify the transient reduction of Cu(II) on a given zeolite, a reference spectrum for the fully Cu(II) state was collected on each sample, taken as the last spectrum recorded at 473 K in the presence of O_2 + NH_3 in order to maintain the sample in the oxidized Cu(II) state. The reference spectrum for the fully Cu(I) state was taken as the average of the last five spectra recorded in the presence of NO + NH_3 at 473 K, which is corroborated by the quantification of 100% Cu(I) from linear-combination fitting of Cu K-edge XANES data collected under the same conditions. The fraction of unreduced Cu(II) as a function of time during each reduction treatment was estimated by integrating the area of the d-d transition band, and linearly interpolating its value between the integrated d-d transition band areas in the spectra for the reference Cu(II) and Cu(I) states.

2.2.3 NH_3 Temperature Programmed Reduction

NH_3-TPR was measured on a Micromeritics Autochem II 2920 Chemisorption analyzer with an online quadrupole mass spectrometer (Cirrus 3, MKS Instruments) tracking NH_3 (m/z = 17), H_2O (m/z = 18), N_2 (m/z = 28), O_2 (m/z = 32), H_2 (m/z = 2), and NO_x products where x=1,2 (m/z = 30, 46). All species except for H_2 were quantified using a Faraday cup detector, while H_2 was quantified using an electron multiplier. The concentration of N_2 was quantified via calibration with a 0.053 kPa N_2/He gas cylinder (533 ppm N_2 UHP, Indiana Oxygen), diluted to varying extents with a second He stream (UHP, Indiana Oxygen) to generate a calibration curve; calibration was performed before and after each NH_3-TPR experiment and the average value between these two measurements was taken as the response factor. The baseline at m/z = 28 was corrected for the presence of background N_2 due to an air leak into the system, as identified by a 4:1 ratio of m/z = 28 and m/z = 32 signals. The concentration of H_2 was quantified via syringe injections of 0.02-0.10 mL of 5 kPa H_2/Ar (5% H_2/Ar, Indiana Oxygen), into a diluent helium stream (50 cm^3 s^{-1}, UHP He, Indiana Oxygen) to generate a response factor, prior to each NH_3-TPR experiment. Integration of the H_2 signal was performed following subtraction of a small, positive baseline.

For a representative NH_3-TPR experiment, 0.027–0.056 g of sieved (180–250 µm) Cu-CHA were loaded into a U-tube quartz reactor with plugs of quartz wool to support the catalyst bed. The sample was first oxidized in air (Zero grade air, Indiana Oxygen; 16.6 cm^3 s^{-1} g^{-1}) to 723 K (0.167 K s^{-1}) for 1 h followed by cooling to 313 K in air. Next, samples were saturated in 0.04 kPa NH_3/He for 2 h at a flow rate of 100 cm^3 s^{-1}, before decreasing the flow rate to 25 cm^3 s^{-1}. The sample temperature was ramped from 313 K to 723 K at a rate of 0.167 K s^{-1} and held at 723 K for 2 h. We verified that no product N_2 is formed on an H-CHA parent sample (Si/Al = 25), and that no additional N_2 is formed upon cooling to 473 K in NH_3 following the TPR on a Cu-CHA sample. H_2O product stoichiometry was not quantified because impurity levels of H_2O were detected in a control NH_3-TPR experiment performed on a H-form zeolite, and a control He TPD experiment on a Cu-form zeolite. NH_3 consumption was not quantified in this TPR experiment because desorption of NH_3 from the sample occurs during the measurement.

2.2.4 *In situ* Cu K-edge X-ray absorption spectroscopy

X-ray absorption spectroscopy experiments were performed at the Advanced Photon Source (APS), Argonne National Laboratory in Lemont, Illinois, in sector 10 Materials Research Collaborative Access Team (MR-CAT). The bending magnet beamline at sector 10 (10-BM) was used for *in situ* experiments. A Cu metal foil reference spectrum (edge energy of 8979 eV) was measured simultaneously with each

sample spectrum collected to calibrate the X-ray beam for spectral measurements at the Cu K-edge. All X-ray absorption near edge structure (XANES) spectra were analyzed in WinXAS and normalized using first and third order polynomials for background subtraction of the pre- and post-edges, respectively. The XANES standards for linear combination fitting (LCF) were collected at the 10-ID beamline with Cu-CHA dehydrated in 21 kPa O_2 (in balance He) at 673 K as a Cu(II) standard and Cu-CHA reduced in 0.03 kPa of NO and NH_3 (balance He, UHP, Indiana Oxygen) at 473 K for the Cu(I) standard.

A "six-shooter" reactor was loaded to contain 5 different Cu-CHA samples that were pelletized and treated simultaneously during each oxidation and reduction treatment. The samples were dehydrated in 10% O_2 (balance He, UHP, Praxair) at 723 K, 10 K min^{-1} for 0.5 h and then cooled to 473 K to collect spectra. Following the oxidation, NH_3 (0.05 kPa in balance He) was introduced to the sample still in the presence of O_2 at 473 K. Spectra were collected until the XANES features stopped changing (deemed to completion). Then the O_2 flow was cut, and *in situ* XANES were collected in the presence of NH_3-only reduction (0.05 kPa, in balance He). Upon completion of NH_3 reduction (deemed when the spectra stopped changing), NO (0.05 kPa) was introduced to the sample to fully reduce to the Cu(I) state.

2.2.5 NO + NH_3 Titration Methods

Reduction of residual Cu(II) sites by 0.03 kPa NO and 0.03 kPa NH_3 (473 K, balance N_2) following treatment in 0.03 kPa NH_3 only (473 K, balance N_2) was performed in a catalytic reactor system described previously for *operando* XAS measurements,[34] modified to use a stainless steel reactor tube for laboratory transient measurements. In a typical titration experiment, 0.020–0.050 g of sieved (180–250 µm) Cu-CHA was loaded in the reactor. Following high-temperature treatment (723 K) in synthetic air (300 cm^3 s^{-1} dry N_2, 75 cm^3 s^{-1} O_2) to prepare the fully oxidized Cu(II) state, the sample was cooled in this gas stream to 473 K. The reactor was purged for 0.17 h with N_2 (340 cm^3 s^{-1} N_2) to remove residual air. Then, NH_3 (0.03 kPa, 3.3 cm^3 s^{-1} of 3.0% NH_3/Ar, Indiana Oxygen) was introduced over the reactor. After a given length of time of Cu(II) exposure to NH_3 only, a pressure-actuated switching valve was used to deliver a mixture of 0.03 kPa NO (3.0 cm^3 s^{-1}, 3.5 % NO/Ar, Indiana Oxygen) and 5 kPa CO_2 (17 cm^3 s^{-1}) over the sample, in addition to the pre-existing NH_3 and N_2 gas streams. Prior to this valve switch, the NO and CO_2 gas mixture (20 cm^3 s^{-1} total flow rate) bypassed the reactor, while a 20 cm^3 s^{-1} "balance N_2" stream flowed to the reactor. After the valve switch, the NO and CO_2 gas mixture replaced the "balance N_2" stream flowing to the reactor, such that the total gas flow rate entering the reactor system remained constant before and after this valve switch. The consumption of NO over time was integrated to calculate the NO/Cu ratio using the CO_2 tracer as a hydrodynamic tracer. Following reduction of Cu(II) by NO and NH_3, the switching valve was cycled to its initial position and then back to its final position to verify that the NO and CO_2 traces were completely overlapped, to assess the validity of using CO_2 as a hydrodynamic tracer. In cases where a small offset between NO and CO_2 traces was observed, the measured NO/Cu value was quantitatively corrected for this error (typically < 0.03 NO/Cu).

In control experiments designed to mitigate the effects of Cu reduction by NH_3 alone, the sample was first exposed to the NO and CO_2 gas mixture prior to NH_3 introduction. Consistent with the literature, NO was not consumed upon introduction of 0.03 kPa NO only.[30] Once the NO signal was stable, the sample was exposed to 0.03 kPa NH_3 which initiated the reduction of Cu(II). The CO_2 tracer accounts for the small change in total gas flow rate upon introduction of the NH_3 stream. In a control experiment involving NO introduction (473 K) following NH_3-TPR, a pre-oxidized Cu-CHA sample was saturated with 0.03 kPa NH_3 (3.0% NH_3/Ar, Indiana Oxygen) at 313 K, heated at 10 K min^{-1} to 693 K, held for 1h, and cooled to 473 K in the same gas mixture. Next, 0.03 kPa NO and CO_2 were introduced, and the NO/Cu ratio was measured to determine the fraction of Cu(II) sites that reduced to Cu(I) in NH_3-only during the TPR.

3. Results and Discussion

3.1 Synthesis of Cu-CHA Zeolites of Varying Cu Speciation

Model Cu-CHA samples with varying Al (Si/Al = 9–25) and Cu (Cu/Al = 0.06–0.37) content were synthesized to contain varying amounts of Z_2Cu and ZCuOH sites, as described in our previous work;[1,2] the salient characterization data summarized in Table 1 (additional characterization data are summarized in Section S.1, SI). Samples are denoted as Cu-CHA(X)-Y where X and Y are the Si/Al and Cu/cage ratios, respectively.

Table 1. Structural and site characterization of Cu-CHA samples.

Sample[a]	Si / Al[b]	Cu /Al[b]	Cu wt%	Cu/cage[c]	Z_2Cu / Al[d]	ZCuOH / Al[d]
Cu-CHA(25)-0.18	25	0.37	1.4	0.18	0.07	0.30
Cu-CHA(9)-0.17	9	0.11	1.3	0.17	0.11	0.00
Cu-CHA(15)-0.14	15	0.18	1.2	0.14	0.10	0.08
Cu-CHA(15)-0.06	15	0.06	0.5	0.05	0.06*	0.00*
Cu-CHA(15)-0.30	15	0.37	2.5	0.30	0.10	0.27

[a] Sample nomenclature is Cu-CHA(X)-Y. X = Si/Al, Y = Cu/cage.

[b] Al content was determined by AAS or ICP and Si content was determined from unit cell of CHA calculations. Uncertainty is ±10%.

[c] Calculated using the fact that CHA zeolites contain 12 T-sites per cage (or 36 T-sites per unit cell).

[d] Determined from a site balance considering total Cu/Al, the number of H^+ titrated on H-form and Cu-form samples, and the 2:1 and 1:1 H^+:Cu exchange stoichiometry expected for Z_2Cu and ZCuOH, respectively.

* Predicted Cu(II) speciation from Co^{2+} saturation,[2] due to large uncertainty in direct quantification from NH_3 TPD given the low Cu content on this sample.

3.2 Titrimetric methods to quantify Cu(II) reduction to Cu(I) during NH_3 treatment

Experimental and computational studies have demonstrated that both mononuclear ZCuOH and Z_2Cu sites reduce in the presence of NO and NH_3, according to Equations (3) and (4), respectively:[1,35,36]

$$Cu(II)OH(NH_3)_3 + NO \rightarrow N_2 + 2H_2O + Cu(I)(NH_3)_2 \quad (3)$$

$$Cu(II)(NH_3)_4 + NO \rightarrow N_2 + H_2O + NH_4^+ + Cu(I)(NH_3)_2 \quad (4)$$

Both of these reaction pathways have a stoichiometry of 1:1:1 NO:Cu:N_2, while the H_2O:Cu stoichiometry depends on the Cu speciation (i.e., Z_2Cu or ZCuOH). Thus, isothermal NO + NH_3 reduction (473 K) was used to quantify the fraction of residual Cu(II) that remained after a pre-reduction treatment in flowing NH_3 for a given time period. This titrimetric method quantifies the extent of Cu(II) reduction independently from measurements of gas-phase product formation stoichiometry (Section 3.4). Control reduction experiments on pre-oxidized (693 K) Cu-CHA samples were performed to expose the sample to NO prior to NH_3 and yielded NO/Cu values of 0.71–1.00, consistent with prior XAS data[3] indicating that these samples contain predominantly ion-exchanged Cu(II). We note that even when NO is introduced prior to NH_3, a fraction of Cu(II) sites may reduce via a pathway involving NH_3 as the sole reductant in parallel with the reduction pathway assisted by NO and NH_3, sometimes leading to NO/Cu values below unity in this experiment.

Cu-CHA samples were exposed to 0.03 kPa NH_3 alone for various periods of time (ca. 2 h, 15 h, and 39 h) at 473 K, prior to introducing NO with an inert CO_2 tracer (profiles in Figs. S3-S4, SI). Figure 1 shows that NH_3 is able to reduce the majority of Cu(II) sites, with similar apparent transient kinetic behavior, on Cu-CHA samples of varying Cu density and speciation. These data indicate that NH_3-assisted reduction occurs on both Z_2Cu and ZCuOH sites, and to qualitatively similar extents as a function of time, irrespective of Cu site speciation or density. After ca. 39 h of NH_3 exposure, the fraction of un-reduced Cu(II) in the Cu-CHA samples studied varied between 0.16–0.23. The Cu-CHA(15)-0.14 sample was further treated for ca. 95 h in NH_3 alone, prior to NO introduction (Fig. 1), which caused the fraction of un-reduced Cu(II) to further decrease to 0.11, suggesting that nearly all Cu(II) ions are able to reduce in NH_3 alone (473 K) given sufficient time.

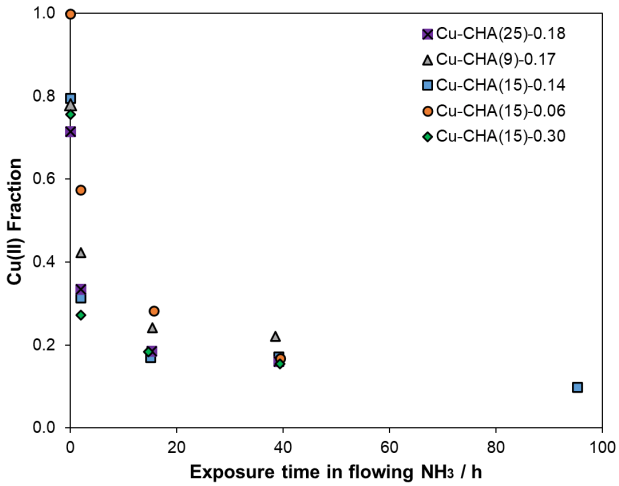

Figure 1. Quantification of the extent of NH_3-only reduction of Cu(II) sites as a function of the NH_3 exposure time at 473 K, determined by titrating residual Cu(II) sites by NO+NH_3 co-reduction, on Cu-CHA samples of varying composition and site type.

3.3 *In situ* XAS and UV-Vis spectroscopy to quantify the extent of Cu(II) reduction

In situ Cu K-edge XANES spectra were collected on representative Cu-CHA samples with varying mononuclear Cu(II) speciation and density (Table 1) upon exposure to two different oxidation treatments (O_2, O_2 + NH_3) and two different reduction treatments (NH_3, NO + NH_3) at 473 K. The XANES spectra collected on Cu-CHA(25)-0.18 after each oxidation or reduction treatment are shown in Figure 2a (spectra on other CHA samples shown in Fig. S12, SI). The features for Cu(I) and Cu(II) are respectively observed at 8.983 keV and 8.987 keV, and the fractions of Cu(I) and Cu(II) were determined from linear combination fitting (LCF) of XANES spectra after each treatment and are listed in Table 2 (additional details in Section S4, SI).

Comparing the two different oxidation treatments, exposure to O_2 alone resulted in complete oxidation of all species to the Cu(II) state (Table 2), while exposure to O_2 + NH_3 resulted in ammonia solvation of the Cu ions along with a small extent of reduction to the Cu(I) state (Fig. 2a, grey dashed spectrum), consistent with observations by Marberger et al.[2,28] O_2 was subsequently removed from the inlet gas stream, and NH_3-only exposure for 11 h (473 K) resulted in further extents of Cu(II) reduction (Fig. 2a, green spectra with darker shades indicating longer exposure time), quantified to result in a Cu(I) fraction of 0.67 (Table 2). XANES spectra measured after analogous treatments on several Cu-CHA samples (Fig. 2b) reveal a similar extent of Cu(II) reduction to Cu(I) after NH_3 treatment (11 h, 473 K). At the end of this NH_3 reduction treatment, the fraction of Cu(I) quantified by XANES was similar on the Cu-CHA samples

studied (0.61–0.73, Table 2), irrespective of mononuclear Cu(II) speciation or density, corroborating the titrimetric data reported in Section 3.2. We note that the hydrodynamics within the *in situ* cell ("six-shooter" reactor) used to collect the XANES spectra in Figure 2 differ from the hydrodynamics of the packed-bed reactor used for the titrimetric methods (Section 3.2) to quantify the transient extent of Cu(II) reduction in NH_3 alone; thus, we did not attempt to quantitatively compare the extent of Cu(II) reduction versus time between these two measurements, although these values are listed in Table 3. After 11 h of NH_3 exposure at 473 K, NO was also introduced into the inlet stream and resulted in nearly complete (80-100%) reduction to the Cu(I) state on all of the Cu-CHA samples studied consistent with *in situ* XANES data reported in prior work;[1–3,27] we note one of the Cu-CHA samples (Cu-CHA(9)-0.17) showed incomplete Cu(II) reduction upon NO + NH_3 exposure at 473 K, which may reflect an artifact caused by sample bypassing within the *in situ* cell ("six-shooter" reactor) used to collect XANES data.

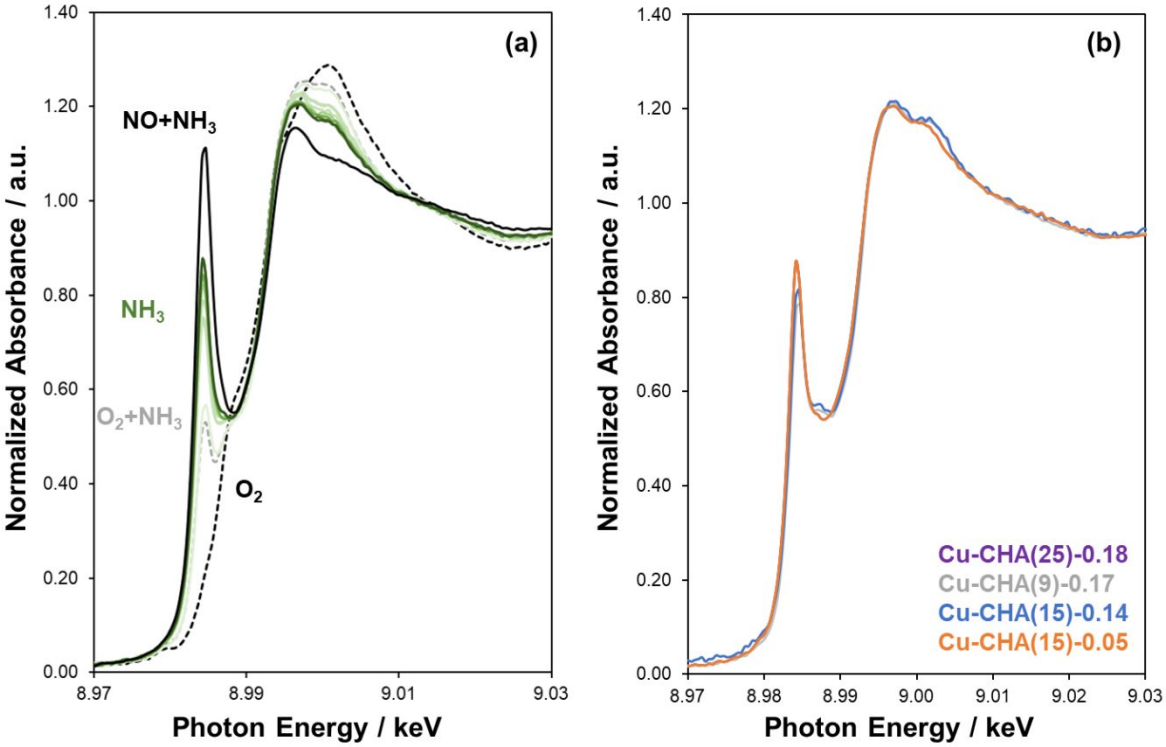

Figure 2. (a) Normalized *in situ* XANES spectra on Cu-CHA(25)-0.18 at 473 K in the presence of (i) O_2 (10 kPa, balance He, black dashed spectrum), (ii) O_2 (10 kPa, balance He) and NH_3 (0.05 kPa, balance He, grey dashed spectrum) (iii), NH_3 (0.05 kPa, balance He, green spectra, darker colors corresponding to longer exposure times), and (iv) NO and NH_3 (0.05 kPa each, balance He, black spectrum). (b) *In situ* XANES spectra for various Cu-CHA samples after exposure to NH_3 for 11 h at 473 K.

Table 2. Cu(II) and Cu(I) distribution determined from LCF analysis of *in situ* XANES spectra on Cu-CHA samples during O_2-only oxidation treatment upon cooling to 473 K (0.5 h), NH_3-only treatment at 473 K (11 h) or NO+NH_3 treatment at 473 K (2 h).

	O_2 Treatment		NH_3-only Treatment		NO+NH_3 Treatment	
Sample	**Cu(I)**	**Cu(II)**	**Cu(I)**	**Cu(II)**	**Cu(I)**	**Cu(II)**
Cu-CHA(25)-0.18	0.03	0.95	0.67	0.33	0.92	0.10
Cu-CHA(9)-0.17	0.02	0.99	0.61	0.39	0.80	0.19
Cu-CHA(15)-0.14	0.00	0.99	0.72	0.29	0.98	0.00
Cu-CHA(15)-0.05	0.01	0.99	0.63	0.38	0.94	0.05

Uncertainty in LCF values for *in situ* XANES is ±10%.

In situ UV-Visible spectra were also collected to corroborate the extent of Cu(II) reduction during NH_3 treatments determined by *in situ* XAS spectroscopy and by NO + NH_3 titrimetric measurements (Section 3.2). Reduction of Cu(II) (d^9) to Cu(I) (d^{10}) results in the disappearance of the d-d transition band (ca. 7,500–20,000 cm^{-1}) in UV-Vis spectra, which has been previously shown using a variety of reductants (NH_3, NO+NH_3, CO, CH_4).[27,37–41] Thus, the integrated area (Kubelka-Munk units) of the d-d transition band on Cu-CHA samples during NH_3 exposure was used as a proxy for the relative proportion of Cu(II) and Cu(I) sites present, and the fractions of Cu(II) and Cu(I) were semi-quantitatively estimated by linear interpolation between the integrated d-d band areas in UV-Vis spectra of these samples collected after O_2 exposure (the predominantly Cu(II) state) and NO + NH_3 exposure (the predominantly Cu(I) state), with the exact Cu(II) and Cu(I) quantities in UV-Vis spectra collected after the O_2 and NO+NH_3 treatments assumed to be equal that quantified by LCF

analysis of *in situ* XANES spectra after equivalent treatments (Table 2).

In situ UV-Visible spectra on representative Cu-CHA samples containing predominantly ZCuOH sites (Cu-CHA(25)-0.18) or predominantly Z_2Cu sites (Cu-CHA(15)-0.05) are respectively shown in Figure 3a and 3b (full range of UV-Vis spectra shown in Figs. S6-S7 and spectra on other Cu-CHA samples shown in Figs. S8-S9, SI), upon exposure to NH_3 with increasing time (473 K) and then exposure to NO + NH_3 (473 K); spectra collected at the end of NO + NH_3 exposure at 473 K shown as black lines. The extent of Cu(II) reduction in the presence of NH_3 alone, and subsequent exposure to NO + NH_3 together, are shown for these two samples in Figures 3c and 3d, respectively, with the vertical dashed line indicating when NO was added to the inlet stream. On both the Cu-CHA(25)-0.18 and Cu-CHA(15)-0.05 samples, exposure to NH_3 causes the Cu(II) fraction to decrease with time to a value of ~0.25 (at 15 h) and ~0.30 (at 20 h) for each sample, respectively. The fraction of Cu(II) remaining at the end of the NH_3 treatment was further decreased with the addition of NO (0.042 kPa) to the inlet stream; at the end of the NO + NH_3 treatment, the small feature that persists in the d-d transition region is reminiscent of the spectrum collected on H-CHA (Fig. S5, SI) and does not reflect a residual fraction of un-reduced Cu(II), given the complete reduction to the Cu(I) state observed by *in situ* XANES (Fig. S12, SI) and in prior reports.[1,3] These semi-quantitative *in situ* UV-Vis data indicate that NH_3-only treatments of Cu-CHA leads to a reduction of Cu(II) content with similar transient behavior, irrespective of mononuclear Cu(II) site speciation (Z_2Cu or ZCuOH), corroborating the conclusions of the quantitative measurements reported using titrimetric methods (Section 3.2).

Table 3. Cu(I) and Cu(II) content quantified during NH_3-only treatment at 473 K using different *in situ* XAS (~11 h of NH_3 exposure), titrimetric methods (~15 h of NH_3 exposure), and *in situ* UV-visible spectroscopy (~20 h of NH_3 exposure).

	In situ XAS		Titrimetric Methods		*In situ* UV-Vis	
Sample	**Cu(I)**	**Cu(II)**	**Cu(I)**	**Cu(II)**	**Cu(I)**	**Cu(II)**

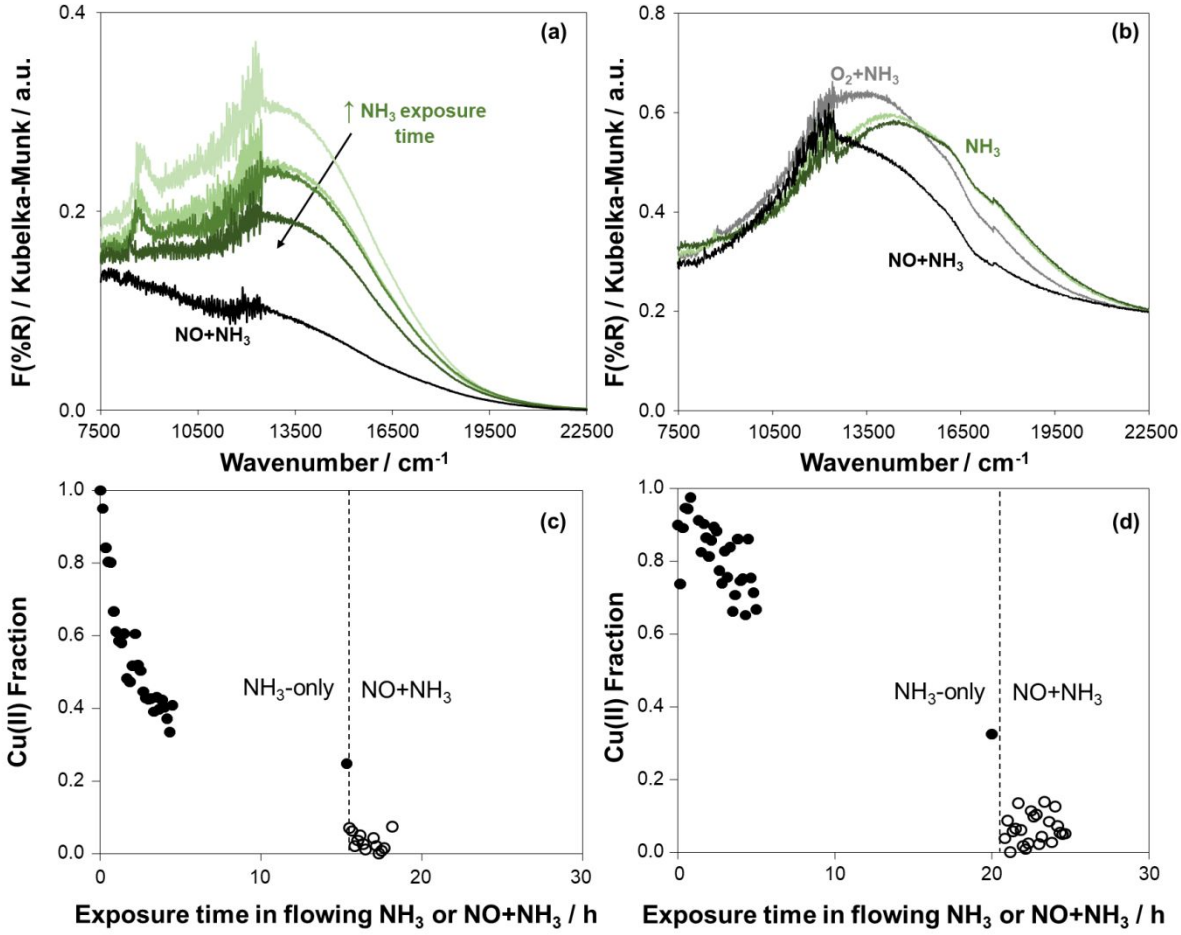

Figure 3. *In situ* UV-Visible spectra (473 K) in the presence of O_2 (21 kPa), NH_3 (0.042 kPa), and balance He at 473 K (dark grey), NH_3 (0.042 kPa, balance He) shown in increasing time from light to dark green, and NO + NH_3 (0.042 kPa each, balance He) shown with black lines on (a) Cu-CHA(25)-0.18 and (b) Cu-CHA(15)-0.05, with quantification of Cu(II) estimated from integrated d-d band areas during transient exposure to NH_3-only (closed) and NO + NH_3 (open) shown in (c) and (d), respectively.

Cu-CHA(25)-0.18	0.67	0.33	0.82	0.18	0.75	0.25
Cu-CHA(9)-0.17	0.61	0.39	0.76	0.24	0.36	0.64
Cu-CHA(15)-0.14	0.72	0.29	0.83	0.17	0.88	0.12
Cu-CHA(15)-0.05	0.63	0.38	0.72	0.28	0.68	0.32

*We note that the hydrodynamics differ within the *in situ* cell ("six-shooter" reactor) used to collect XANES spectra, within the *in situ* UV-Vis diffuse reflectance cell, and within the packed-bed reactor used for the titrimetric methods to quantify the transient extent of Cu(II) reduction in NH_3 alone, which may influence the quantitative comparisons of Cu(II) content among the three methods. The Cu(II) fraction quantified by the NO+NH_3 titrimetric method is the most accurate data set.

3.4 Assessment of NH_3-reduction pathways by monitoring gas phase products during NH_3 TPR

NH_3 TPR was performed on each Cu-CHA sample to identify and quantify the gas-phase reaction products formed, in order to determine a balanced reaction stoichiometry for the NH_3-assisted Cu(II) reduction reaction and assess whether this stoichiometry depends on Cu speciation. N_2 and H_2 were the only gas-phase products quantified during NH_3-TPR and were formed in a similar temperature range of 370–670 K on all samples (Figure 4). N_2 was formed in a stoichiometric ratio with an average value of 0.15 (±0.02) N_2/Cu (Table 4) on all samples, corresponding to an average value of 6.9 (±0.7) Cu(II) ions reduced per N_2 among all of the samples and replicate experiments performed. These results are quantitatively consistent with N_2 formation stoichiometries observed during NH_3 TPD of a Cu-CHA material in a recent report by by Villamaina et al.[42] Other possible products of NH_3 oxidation (NO, NO_2) were not detected by online MS. H_2 was also detected and quantified (H_2/Cu = 0.036–0.097; H_2/N_2 = 0.27–0.65). Given that NH_3 decomposition to N_2 and H_2 should yield a H_2/N_2 ratio of 3, the much lower H_2/N_2 ratios quantified in the effluent gas stream during NH_3 TPR indicate that the equivalent H atoms present in NH_3 are nearly fully (ca. 85%) consumed during the reduction of Cu(II) to Cu(I). It is plausible that H_2 is a reactive intermediate which can reduce distant Cu sites, given that H_2 has been reported as a reductant of Cu(II) to Cu(I) above ca. 423 K,[24,43] alleviating the requirement for multiple Cu(II) ion sites located in close spatial proximity to participate in the NH_3-only reduction process.

To measure the fraction of Cu(II) that reduced during the NH_3-reduction treatment, a NH_3 TPR was carried out on a representative sample (Cu-CHA(15)-0.14), followed by introduction of NO at 473 K. This measurement yielded NO/Cu = 0.05, indicating nearly all (ca. 95%) of the Cu(II) ions present were reduced during the NH_3-TPR measurement, justifying the normalization of N_2 formation stoichiometry by the total Cu content. The measured product N_2 stoichiometry (Table 4) is consistent with a six-electron process whereby two equivalents of NH_3 reduce six Cu(II) ions to Cu(I), to forming one equivalent of N_2:

$$2NH_3 + 6Z_2Cu \rightarrow N_2 + 6ZCu + 6(H^+) \quad (5)$$

$$2NH_3 + 6ZCuOH \rightarrow N_2 + 6ZCu + 6H_2O \quad (6)$$

In the case of Z_2Cu reduction, the H atoms in NH_3 are converted to zeolitic H^+, while in the case of ZCuOH reduction, the H atoms in NH_3 are converted to H_2O; we note that fewer equivalents of H_2O (per Cu) than predicted by Eq. (6) may be formed if proximal ZCuOH sites condense to form ZCuOCuZ species and eliminate H_2O,[8,44,45] prior to NH_3 reduction events. This difference in the fate of H atoms during reduction of Z_2Cu and ZCuOH species is identical to that during Cu(II) reduction to Cu(I) by H_2,[43] and by NO and NH_3 (Eqs. 3-4).[2] The above experimental data and proposed reduction stoichiometry are consistent with a discussion by Dunn et al. on ammonia oxidation on molecular Cu(II) complexes that occur by a six-electron process that results in cleavage of N-H bonds and formation of N-N bonds,[46] but are inconsistent with prior NH_3 TPR measurements that reported a reaction stoichiometry of 1 N_2 per Cu(II) cation on Cu-CHA samples of low Cu density (< 0.3 mmol Cu per g).[31] Such an N_2:Cu stoichiometry would require the formation of 5/2 equivalents of gaseous H_2 per N_2 molecule formed, although H_2 formation was not quantified in this prior work.[31] Our data identify a consistent N_2:Cu stoichiometry across five Cu-CHA samples of varying Cu density and Cu speciation; corroborating quantifications of H_2 formation are consistent with the six-electron redox process described in Eqs. (5) and (6), and inconsistent with a reaction pathway in which 1 N_2 molecule is formed per Cu(II) species reduced.

The above reaction stoichiometry (Eqs. 5-6) involves the reduction of 6 Cu(II) ions by two NH_3 molecules. The N_2/Cu stoichiometry quantified is similar among Cu-CHA samples of varying Cu density and speciation (Table 4). The range of Cu spatial densities studied here corresponds to 0.05–0.30 Cu/cage on average, indicating that most *cha* cages do not contain multiple Cu ions. Thus, the reduction of six equivalents of Cu(II) for every two molecules of NH_3 consumed (and a new N-N bond formed to make N_2) likely occurs via the formation of gaseous reactive intermediates, or via the mobilization of NH_3-solvated Cu complexes,[47] to facilitate the electron transfers required for the overall reactions shown in Equations (5) and (6). This work shows that NH_3 alone reduces nearly all Cu(II) cations to Cu(I) regardless of Cu density and Cu speciation, similarly to NO + NH_3[3,36] or H_2,[24] but contrasting with CO which only reduces ZCuOH sites and not Z_2Cu sites.[48] The contrast between NH_3 and CO as reductants likely results from the different stoichiometric requirements of their oxidation reactions, given that NH_3 is oxidized to N_2 on both ZCuOH and Z_2Cu sites, while oxidation of CO to CO_2 requires extra-lattice oxygen. Overall, these observations motivate future experimental and theoretical work to more precisely understand the elementary step processes that are involved in NH_3-only reduction pathways of Cu(II) ions in Cu-zeolites.

Table 4. Quantification of gas-phase products evolved during NH_3 TPR of Cu-CHA zeolites.

Sample	N_2/Cu^a	Cu/N_2^a	H_2/Cu	H_2/N_2
Cu-CHA(25)-0.18	0.15 (0.13)	6.9 (7.5)	0.048	0.36
Cu-CHA(9)-0.17	0.15 (0.15)	6.7 (6.8)	0.063	0.42
Cu-CHA(15)-0.14	0.16 (0.12)	6.4 (8.0)	0.060	0.48
Cu-CHA(15)-0.05	0.15 (0.18)	6.7 (5.7)	0.097	0.65
Cu-CHA(15)-0.30	0.13 (0.13)	7.7 (7.6)	0.036	0.27

[a]N_2/Cu and Cu/N_2 values in parentheses indicate results from repeat measurements, measured simultaneously with H_2 quantification.

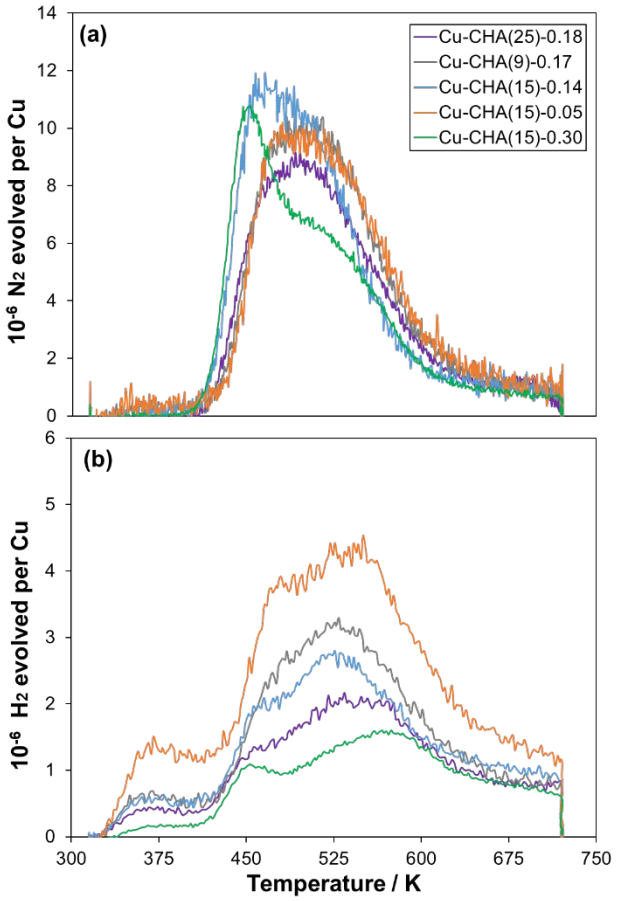

Figure 4. (a) N_2 and (b) H_2 evolution versus temperature during NH_3 TPR on Cu-CHA zeolites.

Conclusions

This work combines spectroscopic, titrimetric, and gas-phase product analysis methods to investigate the NH_3-assisted reduction of mononuclear Cu(II) sites to their Cu(I) states in Cu-CHA zeolites with varying Cu density and speciation (i.e., Z_2Cu and ZCuOH). Titrimetric methods that completely reduce Cu(II) to Cu(I) in flowing NO and NH_3 were used following NH_3-only treatments of Cu-CHA for varying durations of time (473 K), to quantify the transient extent of Cu(II) reduction in the presence of NH_3 alone. These data reveal that Cu(II) ions in Cu-CHA reduce to similar extents as a function of time in NH_3 alone, irrespective of Cu speciation or density. These findings were supported by *in situ* XAS and UV-Visible spectroscopic measurements, which corroborate that both Z_2Cu and ZCuOH-containing Cu-CHA materials show similar extents of Cu(II) reduction during NH_3-only treatments at 473 K.

NH_3 TPR methods were used to quantify gas-phase product formation stoichiometries from reduction of Cu(II) by NH_3 alone, revealing the formation of product N_2 in an approximately 1 N_2 / 6 Cu stoichiometry, irrespective of Cu density or speciation. A small amount of gaseous H_2 was also quantified (H_2/N_2 = 0.27–0.65), but well below the stoichiometry expected from NH_3 decomposition into N_2 and H_2 equivalents (H_2/N_2 = 3), suggesting that H atoms are consumed in the reduction pathway. The fate of the H atoms is expected to depend on the nature of the mononuclear Cu(II) site type, with surface H^+ sites formed upon Z_2Cu reduction or H_2O upon ZCuOH reduction. The observed reaction stoichiometry is consistent with a six-electron reduction process whereby six equivalents of Cu(II) are reduced to Cu(I) upon the consumption of two NH_3 molecules to form one N_2 molecule. These findings illustrate how quantitative titrimetric measurements, in concert with *in situ* spectroscopic interrogation, can provide new insights into the reaction stoichiometry and kinetic behavior associated with reduction processes of transition metal ions exchanged into zeolites.

Given that exposure of Cu-CHA to NH_3 during conditions relevant to NO_x SCR (473 K) results in the reduction of Cu(II) to Cu(I) without the consumption of NO, NH_3-assisted Cu(II) reduction constitutes an undesired side-reaction during NO_x reduction catalysis.[20,24–26] Similar NH_3 and NO conversions are observed at typical conditions of steady-state NO_x SCR catalysis

(e.g., 473 K, 0.03 kPa NO, 0.03 kPa NH_3, 10 kPa O_2) and at differential conversions of NO and NH_3,[23] implying the prevalence of standard SCR pathways (Eq. 1) involving Cu(II) reduction by both NO and NH_3 over Cu(II) reduction pathways by NH_3 only. However, the latter side-reaction may become prevalent at sufficiently high NH_3/NO ratios, such as at high NO conversions given that NH_3 is often supplied at supra-stoichiometric ratios ($NH_3/NO_x > 1$) to facilitate complete NO_x conversion in exhaust aftertreatment systems. Additionally, we note that high temperature (>523 K) reaction conditions, wherein Cu ions are no longer solvated by NH_3 ligands but instead bound to the zeolite in various mononuclear and multinuclear Cu(II) structures, may undergo NH_3-assisted reduction reactions via different mechanisms and kinetic behavior.

This work shows that NH_3-assisted reduction pathways are largely insensitive to changes in mononuclear Cu(II) site type (Z_2Cu and ZCuOH) and Cu density (473 K), implying that such side-reactions occur to similar extents during NO_x SCR catalysis regardless of Cu-zeolite sample composition, and potentially in other zeolite framework topologies prepared to contain predominantly mononuclear Cu(II) ions. This NH_3-assisted reduction pathway may also have implications for Cu-zeolite sample pre-treatments and exposures involving NH_3, whether purposeful or accidental, prior to characterization and quantification techniques. In particular, transient redox experiments involving exposure of Cu(II) species to NH_3 and NO, including spectroscopic (e.g., XAS, UV-Vis), titrimetric (e.g., gas-phase reactant and product quantifications) and reduction kinetics measurements, should be performed with caution to mitigate or otherwise account for the Cu(II) reduction pathway by NH_3 alone that competes with the reduction pathway assisted by NO and NH_3.

Conflicts of interest

There are no conflicts to declare.

Acknowledgements

This study was supported by the U.S. Department of Energy, Office of Science, Office of Basic Energy Sciences, under Award Number DE-SC0019026. Use of the Advanced Photon Source is supported by the U.S. Department of Energy, Office of Science, and Office of Basic Energy Sciences, under Contract no. DE-AC02-06CH11357. MRCAT operations and beamline 10-ID are supported by the Department of Energy and the MRCAT member institutions. We acknowledge Dr. Trevor M. Lardinois and Brandon K. Bolton for helpful technical discussions.

Notes and references

1 C. Paolucci, I. Khurana, A. A. Parekh, S. Li, A. J. Shih, H. Li, J. R. D. Iorio, J. D. Albarracin-Caballero, A. Yezerets, J. T. Miller, W. N. Delgass, F. H. Ribeiro, W. F. Schneider and R. Gounder, *Science*, 2017, **357**, 898–903.

2 C. Paolucci, A. A. Parekh, I. Khurana, J. R. Di Iorio, H. Li, J. D. Albarracin Caballero, A. J. Shih, T. Anggara, W. N. Delgass, J. T. Miller, F. H. Ribeiro, R. Gounder and W. F. Schneider, *J. Am. Chem. Soc.*, 2016, **138**, 6028–6048.

3 C. B. Jones, I. Khurana, S. H. Krishna, A. J. Shih, W. N. Delgass, J. T. Miller, F. H. Ribeiro, W. F. Schneider and R. Gounder, *Journal of Catalysis*, 2020, **389**, 140–149.

4 G. Brezicki, J. D. Kammert, T. B. Gunnoe, C. Paolucci and R. J. Davis, *ACS Catal.*, 2019, **9**, 5308–5319.

5 D. Bregante, L. Wilcox, C. Liu, C. Paolucci, R. Gounder and D. Flaherty, *ACS Catal.*, 2021, **11**, 11873–11884.

6 E. M. C. Alayon, M. Nachtegaal, A. Bodi, M. Ranocchiari and J. A. van Bokhoven, *Phys. Chem. Chem. Phys.*, 2015, **17**, 7681–7693.

7 S. Grundner, M. A. C. Markovits, G. Li, M. Tromp, E. A. Pidko, E. J. M. Hensen, A. Jentys, M. Sanchez-Sanchez and J. A. Lercher, *Nature Communications*, 2015, **6**, 7546.

8 B. Ipek, M. J. Wulfers, H. Kim, F. Göltl, I. Hermans, J. P. Smith, K. S. Booksh, C. M. Brown and R. F. Lobo, *ACS Catal.*, 2017, **7**, 4291–4303.

9 K. Narsimhan, K. Iyoki, K. Dinh and Y. Román-Leshkov, *ACS Cent. Sci.*, 2016, **2**, 424–429.

10 K. T. Dinh, M. M. Sullivan, K. Narsimhan, P. Serna, R. J. Meyer, M. Dinca and Y. Roman-Leshkov, *J. Am. Chem. Soc.*, , DOI:10.1021/jacs.9b04906.

11 K. T. Dinh, M. M. Sullivan, P. Serna, R. J. Meyer, M. Dincă and Y. Román-Leshkov, *ACS Catal.*, 2018, **8**, 8306–8313.

12 E. M. Alayon, M. Nachtegaal, M. Ranocchiari and J. A. van Bokhoven, *Chem. Commun.*, 2011, **48**, 404–406.

13 N. V. Beznis, B. M. Weckhuysen and J. H. Bitter, *Catal Lett*, 2010, **138**, 14–22.

14 E. Borfecchia, K. A. Lomachenko, F. Giordanino, H. Falsig, P. Beato, A. V. Soldatov, S. Bordiga and C. Lamberti, *Chem. Sci.*, 2014, **6**, 548–563.

15 R. Gounder and A. Moini, *React. Chem. Eng.*, 2019, **4**, 966–968.

16 C. H. F. Peden, *Journal of Catalysis*, 2019, **373**, 384–389.

17 C. K. Lambert, *React. Chem. Eng.*, 2019, **4**, 969–974.

18 H. Lee, I. Song, S. Won Jeon and D. Heui Kim, *Catalysis Science & Technology*, 2021, **11**, 4838–4848.

19 G. Cavataio, J. Girard, J. E. Patterson, C. Montreuil, Y. Cheng and C. K. Lambert, 2007, pp. 2007-01–1575.

20 F. Gao, E. D. Walter, M. Kollar, Y. Wang, J. Szanyi and C. H. F. Peden, *Journal of Catalysis*, 2014, **319**, 1–14.

21 T. V. W. Janssens, H. Falsig, L. F. Lundegaard, P. N. R. Vennestrøm, S. B. Rasmussen, P. G. Moses, F. Giordanino, E. Borfecchia, K. A. Lomachenko, C. Lamberti, S. Bordiga, A. Godiksen, S. Mossin and P. Beato, *ACS Catal.*, 2015, **5**, 2832–2845.

22 K. A. Lomachenko, E. Borfecchia, C. Negri, G. Berlier, C. Lamberti, P. Beato, H. Falsig and S. Bordiga, *J. Am. Chem. Soc.*, 2016, **138**, 12025–12028.

23 S. A. Bates, A. A. Verma, C. Paolucci, A. A. Parekh, T. Anggara, A. Yezerets, W. F. Schneider, J. T. Miller, W. N. Delgass and F. H. Ribeiro, *Journal of Catalysis*, 2014, **312**, 87–97.

24 F. Gao, N. M. Washton, Y. Wang, M. Kollár, J. Szanyi and C. H. F. Peden, *Journal of Catalysis*, 2015, **331**, 25–38.

25 M. Jabłońska, *ChemCatChem*, 2020, **12**, 4490–4500.

26 C. Paolucci, J. R. Di Iorio, F. H. Ribeiro, R. Gounder and W. F. Schneider, in *Advances in Catalysis*, ed. C. Song, Academic Press, 2016, vol. 59, pp. 1–107.

27 E. Borfecchia, C. Negri, K. A. Lomachenko, C. Lamberti, T. V. W. Janssens and G. Berlier, *React. Chem. Eng.*, 2019, **4**, 1067–1080.

28 A. Marberger, A. W. Petrov, P. Steiger, M. Elsener, O. Kröcher, M. Nachtegaal and D. Ferri, *Nat Catal*, 2018, **1**, 221–227.
29 C. Liu, H. Kubota, T. Amada, T. Toyao, Z. Maeno, M. Ogura, N. Nakazawa, S. Inagaki, Y. Kubota and K. Shimizu, *Catalysis Science & Technology*, 2021, **11**, 4459–4470.
30 C. Paolucci, A. A. Verma, S. A. Bates, V. F. Kispersky, J. T. Miller, R. Gounder, W. N. Delgass, F. H. Ribeiro and W. F. Schneider, *Angewandte Chemie International Edition*, 2014, **53**, 11828–11833.
31 Y. Ma, X. Wu, J. Ding, L. Liu, B. Jin, E. Walter, R. Ran, Z. Si, F. Gao and D. Weng, *Chem. Commun.*, , DOI:10.1039/D0CC07346F.
32 M. Moreno-González, B. Hueso, M. Boronat, T. Blasco and A. Corma, *J. Phys. Chem. Lett.*, 2015, **6**, 1011–1017.
33 J. R. Di Iorio and R. Gounder, *Chem. Mater.*, 2016, **28**, 2236–2247.
34 V. F. Kispersky, A. J. Kropf, F. H. Ribeiro and J. T. Miller, *Phys. Chem. Chem. Phys.*, 2012, **14**, 2229–2238.
35 W. Hu, T. Selleri, F. Gramigni, E. Fenes, K. R. Rout, S. Liu, I. Nova, D. Chen, X. Gao and E. Tronconi, *Angewandte Chemie*, 2021, **60**, 7197–7204.
36 R. Villamaina, S. Liu, I. Nova, E. Tronconi, M. P. Ruggeri, J. Collier, A. York and D. Thompsett, *ACS Catal.*, 2019, **9**, 8916–8927.
37 F. Giordanino, P. N. R. Vennestrøm, L. F. Lundegaard, F. N. Stappen, S. Mossin, P. Beato, S. Bordiga and C. Lamberti, *Dalton Trans.*, 2013, **42**, 12741–12761.
38 H. Li, C. Paolucci, I. Khurana, L. N. Wilcox, F. Göltl, J. D. Albarracin-Caballero, A. J. Shih, F. H. Ribeiro, R. Gounder and W. F. Schneider, *Chem. Sci.*, 2019, **10**, 2373–2384.
39 R. Oord, J. E. Schmidt and B. M. Weckhuysen, *Catalysis Science & Technology*, 2018, **8**, 1028–1038.
40 V. L. Sushkevich, M. Artsiusheuski, D. Klose, G. Jeschke and J. A. van Bokhoven, *Angewandte Chemie International Edition*, 2021, **60**, 15944–15953.
41 J. S. Woertink, P. J. Smeets, M. H. Groothaert, M. A. Vance, B. F. Sels, R. A. Schoonheydt and E. I. Solomon, *Proc. Natl. Acad. Sci. U.S.A.*, 2009, **106**, 18908–18913.
42 R. Villamaina, F. Gramigni, U. Iacobone, S. Liu, I. Nova, E. Tronconi, M. P. Ruggeri, J. Collier, A. P. E. York and D. Thompsett, *Catalysts*, 2021, **11**, 759.
43 P. D. Costa, B. Modén, G. D. Meitzner, D. Ki Lee and E. Iglesia, *Physical Chemistry Chemical Physics*, 2002, **4**, 4590–4601.
44 V. L. Sushkevich, A. V. Smirnov and J. A. van Bokhoven, *J. Phys. Chem. C*, 2019, **123**, 9926–9934.
45 V. L. Sushkevich and J. van Bokhoven, *Chem. Commun.*, 2018, **54**, 7447–7450.
46 P. L. Dunn, B. J. Cook, S. I. Johnson, A. M. Appel and R. M. Bullock, *Journal of the American Chemical Society*, 2020, **142**, 17845–17858.
47 C. Paolucci, J. R. Di Iorio, W. F. Schneider and R. Gounder, *Acc. Chem. Res.*, 2020, **53**, 1881–1892.
48 R. Villamaina, U. Iacobone, I. Nova, E. Tronconi, M. P. Ruggeri, J. Collier and D. Thompsett, *ChemCatChem*, 2020, **12**, 3843–3848.